Control Engineering Practice 18 (2010) 1357–1368

Contents lists available at ScienceDirect

Control Engineering Practice

journal homepage: www.elsevier.com/locate/conengprac

Comparison between linear and nonlinear control strategies for variable speed wind turbines

B. Boukhezzar *, H. Siguerdidjane **

Automatic Control Department, Supélec, Plateau du Moulon, 3, rue Joliot-Curie, 91192 Gif-sur-Yvette cedex, France

ARTICLE INFO

Article history:
Received 9 April 2009
Accepted 28 June 2010

Keywords:
LQG control
Nonlinear control
Renewable energies
Two-mass model
Variable speed wind turbines

ABSTRACT

The purpose of this work is to compare some linear and nonlinear control strategies, with the aim of benefiting as well as possible of wind energy conversion systems. Below rated wind speed, the main control objective is to perform an optimal wind power capture while avoiding strong loads on the drive train shafts. To explicitly take into consideration the low speed shaft flexibility, a two-mass nonlinear model of the wind turbine is used for controllers synthesis. After adapting a LQG controller based on the linearized model, nonlinear controllers based on a wind speed estimator are developed. They take into account the nonlinear dynamic aspect of the wind turbine and the turbulent nature of the wind. The controllers are validated upon an aeroelastic wind turbine simulator for a realistic wind speed profile. The study shows that nonlinear control strategies bring more performance in the exploitation of wind energy conversion systems.

1. Introduction

In the perspective of wind energy electric power production increasing, it is crucial to optimize wind energy conversion systems (WECS) exploitation. Efficient production tools and methods are then necessary. Even if they are less implemented and more complicated to be controlled, variable speed wind turbines (VSWT) show many advantages compared to fixed speed wind turbines (Ernst & Leonhard, 1985; Vihriälä, 2002). Their annual production exceeds the fixed speed ones by 5–10%. For this kind of turbines, it is shown that the action of the control system can have a major impact on the loads submitted by the turbine (Bianchi, Battista, & Mantz, 2006; Heier, 1998). The design of the controller must take into account the effect on loads, and at least ensure that excessive loads will not result from the control action (Burton, Sharpe, Jenkins, & Bossanyi, 2001; Munteanu, Bratcu, Cutululis, & Ceang, 2008). Many of the wind turbines control systems are based on linear models. This is due to several reasons. On the one hand, there are generally simple analytical solutions to many control problems (LQR, pole-placement, Kalman-filtering). On the other hand, it is easier to implement such controllers in practical applications. Indeed, and until now, the major part of implemented wind turbine controllers are based on linearized models (Bianchi, Mantz, & Christiansen, 2005; Bongers, Bierbooms, Dijkstra, & van Hoten, 1990; Ekelund & Schmidtbauer, 1993; Munteanu, Cutululis, Iuliana, & Ceanga, 2005).

Wind turbine controller objectives depend on the operating area (Boukhezzar, Lupu, Siguerdidjane, & Hand, 2007; Camblong, 2008). For low wind speeds, it is more important to optimize wind power capture. Above the rated power, the primary objective of the controllers is to reduce electrical power and rotor speed fluctuations while minimizing the control actuating loads. When the wind speed exceeds its nominal value, the control objective shifts from maximizing power capture to regulating power to the turbine's rated output. Two control inputs are then available: the generator torque and the blade pitch angle. Linear controllers have been extensively used for power regulation through the control of blade pitch angle. A review of the main control methods is given in Boukhezzar et al. (2007). The performance of the linear controllers is limited by the highly nonlinear characteristics of the wind turbine. Typical power regulation control schemes use blade pitch angle as the only controller input. The Generator torque is sometimes controlled according to the method employed for the below-rated wind speed conditions known as the indirect control in torque technique. Most controllers hold the generator torque constant at its nominal value making the controller monovariable in pitch only (Van der Hooft & Van Engelen, 2003, 2004). These monovariable controllers are unable to meet the multiple objectives of regulating the electrical power and rotor speed. A multivariable controller for power control above rated was proposed in a previous work (Boukhezzar et al., 2007).

The objective of this paper is to design a controller, for power capture optimization, that takes into consideration the nonlinear nature of the wind turbine behavior, the flexibility of the drive-train shaft and the turbulent nature of the wind. These aspects are

* Principal Corresponding author. Tel.: +33 1 69 85 1372; fax: +33 1 69 85 1389.
** Corresponding author. Tel.: +33 1 69 85 1377; fax: +33 1 69 85 13 89.
E-mail addresses: boubekeur.boukhezzar@supelec.fr (B. Boukhezzar), houria.siguerdidjane@supelec.fr (H. Siguerdidjane).

0967-0661/$ - see front matter © 2010 Published by Elsevier Ltd.
doi:10.1016/j.conengprac.2010.06.010

Nomenclature

v	wind speed, m s^{-1}
ρ	air density, kg m^{-3}
R	rotor radius, m
P_a	aerodynamic power, W
T_a	aerodynamic torque, N m
P_e	electrical power, W
λ	tip speed ratio
β	pitch angle, deg
$C_p(\lambda,\beta)$	power coefficient
$C_q(\lambda,\beta)$	torque coefficient
ω_t	rotor speed, rad s^{-1}
ω_g	generator speed, rad s^{-1}
ω_{ls}	low speed shaft speed, rad s^{-1}
θ_t	rotor side angular deviation, rad
θ_{ls}	gearbox side angular deviation, rad
θ_g	generator side angular deviation, rad
T_{em}	generator (electromagnetic) torque, N m
T_{ls}	low speed shaft torque, N m
T_{hs}	high speed shaft torque, N m
J_r	rotor inertia, kg m^2
J_g	generator inertia, kg m^2
B_r	rotor external damping, N m rad^{-1} s^{-1}
B_g	generator external damping, N m rad^{-1} s^{-1}
B_{ls}	low speed shaft damping, N m rad^{-1} s^{-1}
K_{ls}	low speed shaft stiffness, N m rad^{-1}
$\hat{x}$	estimate of x
$\dot{x},\ddot{x}$	first and second derivative of x with respect to time
$x^{(i)}$	ith derivative of x with respect to time
x_{opt}	optimal value of x
WT	wind turbine
NREL	national renewable energy laboratory
CART	controls advanced research turbine
FAST	fatigue, aerodynamics, structures, and turbulence
LQG	linear quadratic Gaussian
NSSFE	nonlinear static state feedback with estimator
NDSFE	nonlinear dynamic state feedback with estimator

considered in previous works, but not simultaneously. Linear controllers based on the two-mass wind turbine model were proposed in Bianchi et al. (2006), Ekelund (1997) and Bongers (1994). Nonlinear controllers with wind speed estimators have also been proposed using a one-mass model (Boukhezzar, Siguerdidjane, & Hand, 2006). Hence, in this work, it is proposed to extend this method using a two-mass model of the drive train. This is motivated by the fact that the one mass-model cannot report the flexibility of the low speed shaft. However, this flexibility induces flexible resonant and non-resonant modes that can cause system oscillations.

The contribution of this work, with regard to the literature, is on the one hand the consideration of a two-mass model for nonlinear controllers synthesis. On the other hand, the contribution of this work consists of proposing controllers that take into consideration the nonlinear nature of the wind turbine aerodynamics, its flexible structure, using a two-mass model and the wind turbulence nature without considering that this one is measurable. The nonlinear controllers use nonlinear static and dynamic state feedback, with a wind speed estimator, to track the optimal tip speed ratio. The wind speed is estimated using the wind turbine itself as a measurement device. The proposed nonlinear controllers avoid the assumptions that the wind speed is measurable or that the WT evolves near an operating point that allows the use of a local linearized model. This paper is organized as follows: in Section 2, after a brief presentation of the aerodynamic model, the two-mass model is given in a state-space form. A background of WT control objectives in low speed areas is given in Section 3. LQG controller is then deduced in Section 4 from the linearized model in the aim of satisfying a trade-off between wind power capture optimization and drive train load reduction. The wind speed estimator is presented in Section 5. To overcome the limited performance of the linear controller, nonlinear controllers based on the two-mass nonlinear wind turbine model and using the wind speed estimator are presented in Section 6. The controllers are coupled with a wind speed estimator. In Section 7, the developed controllers are validated upon an aeroelastic wind turbine simulator for a realistic high-turbulence wind speed profile under some constraints (input perturbation and measurement noise). The simulation results show a better performance for the nonlinear controller regarding wind power capture while standing in acceptable control loads and drive train torque transient loads.

2. Wind turbine modelling

A two-mass model is commonly used in the literature (Bongers, 1994; Novak et al., 1994; Sørensen, Hansen, Janosi, Bech, & Bak-Jensen, 2001) to describe the wind turbine dynamics. Its scheme is illustrated in Fig. 1(a).

The use of a two-mass model for controllers synthesis is motivated by the fact that the control laws derived from this model are more general and can be applied for wind turbines of different sizes. Particularly, these controllers are more adapted for high-flexibility wind turbines that cannot be properly modelled with a one mass model (Boukhezzar et al., 2006). In fact, it is also shown in Ma (1997) that the two-mass model can report flexible modes in the drive train model that cannot be highlighted with the one mass model.

The aerodynamic power captured by the rotor is given by

$$P_a = \tfrac{1}{2}\rho\pi R^2 C_p(\lambda,\beta)v^3 \tag{1}$$

The power coefficient C_p depends on the blade pitch angle β and the tip speed ratio λ is defined as

$$\lambda = \frac{\omega_t R}{v} \tag{2}$$

the aerodynamic torque is

$$T_a = \tfrac{1}{2}\rho\pi R^3 C_q(\lambda,\beta)v^2 \tag{3}$$

where

$$C_q(\lambda,\beta) = \frac{C_p(\lambda,\beta)}{\lambda} \tag{4}$$

is the torque coefficient. The list of symbols used in this paper is given in the beginning of the revised paper.

The rotor-side inertia J_r dynamics are given by the first order differential equation

$$J_r\dot{\omega}_t = T_a - T_{ls} - B_r\omega_t \tag{5}$$

the low-speed shaft torque T_{ls} acts as a braking torque on the rotor

$$T_{ls} = K_{ls}(\theta_t - \theta_{ls}) + B_{ls}(\omega_t - \omega_{ls}) \tag{6}$$

The generator inertia J_g is driven by the high-speed shaft and braked by the electromagnetic torque T_{em}

$$J_g\dot{\omega}_g = T_{hs} - B_g\omega_g - T_{em} \tag{7}$$

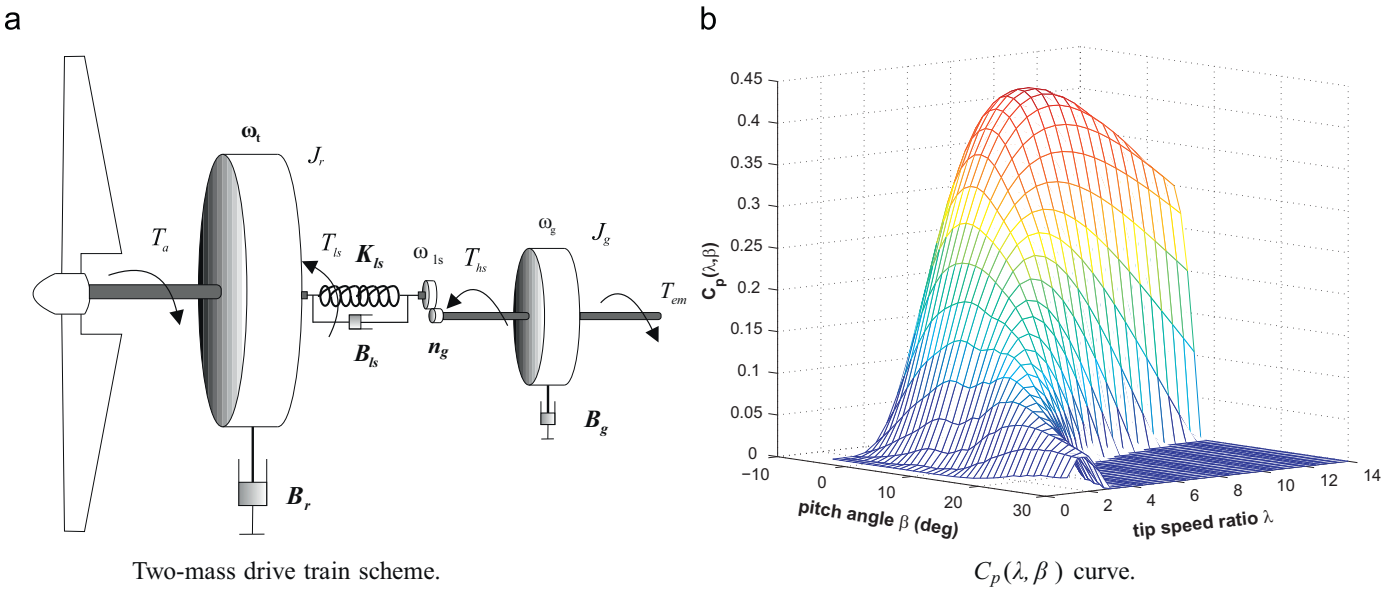

Fig. 1. Two-mass wind turbine model characteristics. (a) Two-mass drive train scheme. (b) $C_p(\lambda,\beta)$ curve.

If an ideal gearbox with a ratio n_g is assumed, one has

$$n_g = \frac{T_{ls}}{T_{hs}} = \frac{\omega_g}{\omega_{ls}} = \frac{\theta_g}{\theta_{ls}} \tag{8}$$

deducing T_{ls} time derivative from (6) and using (7) and (8) leads to the following dynamic system:

$$\begin{bmatrix} \dot{\omega}_t \\ \dot{\omega}_g \\ \dot{T}_{ls} \end{bmatrix} = \begin{bmatrix} a_{11} & a_{12} & a_{13} \\ a_{21} & a_{22} & a_{23} \\ a_{31} & a_{32} & a_{33} \end{bmatrix} \begin{bmatrix} \omega_t \\ \omega_g \\ T_{ls} \end{bmatrix} + \begin{bmatrix} b_{11} \\ b_{21} \\ b_{31} \end{bmatrix} T_a + \begin{bmatrix} b_{12} \\ b_{22} \\ b_{32} \end{bmatrix} T_{em} \tag{9}$$

where

$$a_{11} = -\frac{B_r}{J_r}, \quad a_{12} = 0, \quad a_{13} = -\frac{1}{J_r}$$

$$a_{21} = 0, \quad a_{22} = -\frac{B_g}{J_g}, \quad a_{23} = \frac{1}{n_g J_g}$$

$$a_{31} = \left(K_{ls} - \frac{B_{ls}B_r}{J_r}\right), \quad a_{32} = \frac{1}{n_g}\left(\frac{B_{ls}B_r}{J_g} - K_{ls}\right)$$

$$a_{33} = -B_{ls}\left(\frac{J_r + n_g^2 J_g}{n_g^2 J_g J_r}\right)$$

and

$$b_{11} = \frac{1}{J_r}, \quad b_{12} = 0$$

$$b_{21} = 0, \quad b_{22} = -\frac{1}{J_g}$$

$$b_{31} = \frac{B_{ls}}{J_r}, \quad b_{22} = \frac{B_{ls}}{n_g J_g}$$

3. Control objectives

One can distinguish two operating areas of a variable speed wind turbine: below and above the rated wind speed.

Below the nominal power, the main control objectives are (Ekelund & Schmidtbauer, 1994):

1. Maximize wind power capture.
2. Reduce loads submitted by the drive train shaft.

The power coefficient curve $C_p(\lambda,\beta)$ has a unique maximum that corresponds to an optimal wind energy capture (Fig. 1(b)).

$$C_p(\lambda_{opt},\beta_{opt}) = C_{p_{opt}} \tag{10}$$

where

$$\lambda_{opt} = \frac{\omega_{topt} R}{v} \tag{11}$$

Consequently, in partial load operating mode, in order to maximize wind power extraction, the blade pitch angle is fixed to its optimal value β_{opt} and with the aim of maintaining λ at its optimal value, the rotor speed ω_t must be adjusted to track the optimal reference given by

$$\omega_{t_{opt}} = \frac{\lambda_{opt}}{R} v \tag{12}$$

The WT electric system time responses are much faster than those of the other parts of the WT. This makes it possible to dissociate the generator and the aeroturbine (mechanical and aerodynamic part) control designs and thus define a cascaded control structure around two control loops.

1. The inner control loop concerns the electric generator via the power converters.
2. The outer control loop concerns the aeroturbine that provides the reference inputs of the inner loop.

Many other works address the electrical part control without considering the aeroturbine control (Ekanayake, Holdsworth, Wu, & Jenkins, 2003). Making the assumption that the internal (electrical) loop is well controlled, this work focus on the aeroturbine control. Other controllers have been proposed in previous works considering the control of the whole system (Boukhezzar & M'Saad, 2008; Boukhezzar & Siguerdidjane, 2009).

4. LQG control

Given the diversity of available methods, it is more common to synthesize wind turbine controllers from the linearized model for an operating point corresponding to the mean wind speed.

The linear quadratic Gaussian (LQG) control technique has proven to be efficient in the control of many important

applications (Burns, 2001). A LQG controller is composed of a linear quadratic regulator (LQR) together with a Kalman filter state estimator. The LQR regulator provides an optimal control law for a linear system (A,B,C) with a quadratic performance index J

$$J=\int_{t_0}^{t_1}(\boldsymbol{x}^T\boldsymbol{Q}\boldsymbol{x}+\boldsymbol{u}^T\boldsymbol{R}\boldsymbol{u})\,\mathrm{d}t \tag{13}$$

When t_1 is infinite, or far removed from t_0, the optimal control law is given by (Burns, 2001)

$$u_{opt}=-\boldsymbol{R}^{-1}\boldsymbol{B}^T\boldsymbol{P}\boldsymbol{x} \tag{14}$$

where $\boldsymbol{P}$ matrix is the solution of the algebraic Riccati equation

$$\boldsymbol{P}\boldsymbol{A}+\boldsymbol{A}^T\boldsymbol{P}+\boldsymbol{Q}-\boldsymbol{P}\boldsymbol{B}\boldsymbol{R}^{-1}\boldsymbol{B}^T\boldsymbol{P}=0 \tag{15}$$

The Kalman estimator coupled with the LQR controller extracts the best estimate of the state variables from a number of measurements that contain a white Gaussian noise. It is based on the minimization of the estimation error variance. For more details about Kalman filter and LQR/LQG controllers, the readers are referred to Anderson and Moore (1989), Burns (2001) and Lin (2007). The LQG controller proposed in this section is inspired from Ma (1997) and adapted to the two-mass model herein considered. For this, the WT model is firstly linearized.

4.1. Model linearization

As shown in (3), the nonlinear nature of WT dynamic model comes from the aerodynamic torque. T_a depends on the rotor speed ω_t, the blade pitch angle and the wind speed v that is a random highly fluctuating uncommendable input. Linearizing the aerodynamic torque for a given operating point leads to the following expression:

$$\begin{aligned}T_a&=T_{a_0}+\Delta T_a\\&=T_{a_0}+\alpha\Delta v+\gamma\Delta\omega_t+\delta\Delta\beta\end{aligned} \tag{16}$$

where α, γ and δ are constant coefficients. New state variables corresponding to the variations around the operating point are then defined

$$\begin{aligned}&v'=\Delta v=v-v_0\\&\omega_t{}'=\Delta\omega_t=\omega_t-\omega_{t_0}\\&\omega_g{}'=\Delta\omega_g=\omega_g-\omega_{g_0}\\&T_{ls}{}'=\Delta T_{ls}=T_{ls}-T_{ls_0}\\&T_{em}{}'=\Delta T_{em}=T_{em}-T_{em_0}\\&\beta'=\Delta\beta=\beta-\beta_0\end{aligned} \tag{17}$$

For low wind speeds, the blade pitch angle is fixed ($\Delta\beta=0$). The WT model is then a SISO system where the generator torque constitutes the input and the rotor speed ω_t the output. The aerodynamic torque expression is then

$$T_a{}'=\alpha v'+\gamma\omega_t{}' \tag{18}$$

In this case, the linearized state space model is

$$\begin{aligned}&\dot{\boldsymbol{x}}=\boldsymbol{A}\boldsymbol{x}+\boldsymbol{B}_1T_{em}{}'+\boldsymbol{B}'v'\\&y=\boldsymbol{C}\boldsymbol{x}\end{aligned} \tag{19}$$

with

$$\boldsymbol{x}=[\omega_t{}'\ \ \omega_g{}'\ \ T_{ls}{}']^T,\quad y=\omega_g{}'$$

The state-space model matrices are given in (20):

$$\boldsymbol{A}=\begin{bmatrix}\frac{\gamma-B_r}{J_r} & 0 & \frac{1}{J_r}\\ 0 & -\frac{B_g}{J_g} & \frac{1}{n_gJ_g}\\ (K_{ls}-\frac{B_{ls}B_r}{J_r})+\frac{\gamma B_{ls}}{J_r} & \frac{1}{n_g}(\frac{B_{ls}B_g}{J_g}-K_{ls}) & -B_{ls}(\frac{J_r+n_g^2J_g}{n_g^2J_gJ_r})\end{bmatrix},\ \boldsymbol{B}_1=\begin{bmatrix}0\\-\frac{1}{J_g}\\\frac{B_{ls}}{n_gJ_g}\end{bmatrix}$$

$$\boldsymbol{B}'=\begin{bmatrix}\frac{\alpha}{J_r}\\0\\\frac{\alpha B_{ls}}{J_r}\end{bmatrix},\quad \boldsymbol{C}=[0\ \ 1\ \ 0] \tag{20}$$

Assimilating the wind speed v' to a linear filtered non-correlated white noise, one can write

$$\begin{aligned}&\dot{\boldsymbol{x}}_v=\boldsymbol{A}_v\boldsymbol{x}_v+\boldsymbol{B}_ve_v\\&v'=\boldsymbol{C}_v\boldsymbol{x}_v\end{aligned} \tag{21}$$

where $\boldsymbol{A}_v$,$\boldsymbol{B}_v$ and $\boldsymbol{C}_v$ depend on the mean wind speed, ground characteristics and wind speed assumed turbulence (Ma, 1997). e_v is a unity variance non-correlated white-noise.

Finally, the whole state-space representation of the linearized model is

$$\begin{bmatrix}\dot{\boldsymbol{x}}\\\dot{\boldsymbol{x}}_v\end{bmatrix}=\begin{bmatrix}\boldsymbol{A} & \boldsymbol{B}'\boldsymbol{C}_v\\\boldsymbol{0} & \boldsymbol{A}_v\end{bmatrix}\begin{bmatrix}\boldsymbol{x}\\\boldsymbol{x}_v\end{bmatrix}+\begin{bmatrix}\boldsymbol{B}_1\\\boldsymbol{0}\end{bmatrix}T_{em}{}'+\begin{bmatrix}\boldsymbol{0}\\\boldsymbol{B}_v\end{bmatrix}e_v \tag{22}$$

4.2. LQG controller synthesis

The wind power capture optimization and load torque fluctuation reduction objectives can be simultaneously taken into account by minimizing the criterion J_{bel} (Ma, 1997)

$$J_{bel}=\lim_{T\to\infty}\frac{1}{T}E\left\{\int_0^T(Q_a\Delta P_a+Q_t(\Delta T_{em})^2)\,\mathrm{d}t\right\} \tag{23}$$

Q_a and Q_t are the weighting factors. It is shown in Ma (1997) that the minimization of (23) is equivalent to minimizing the following criterion:

$$J_{bel}=\lim_{T\to\infty}\frac{1}{T}E\left\{\int_0^T(\boldsymbol{x}_a^T\boldsymbol{Q}_{x_a}\boldsymbol{x}_a+Q_t(\Delta T_{em})^2)\,\mathrm{d}t\right\} \tag{24}$$

where

$$\boldsymbol{Q}_{x_a}=\boldsymbol{H}^TQ_l\boldsymbol{H}\quad\text{with } Q_l=\tfrac{1}{2}\rho\pi R^2v_0^3c_0Q_a$$

and

$$\boldsymbol{H}=\left[\left.\frac{\partial\lambda}{\partial\omega_t}\right|_{op}\ 0\ 0\ \left.\frac{\partial\lambda}{\partial v}\right|_{op}\ 0\right]$$

$$\boldsymbol{x}_a=[\omega_t{}'\ \ \omega_g{}'\ \ T_{ls}{}'\ \ v'\ \ \dot{v}']^T$$

In order to achieve a compromise between aerodynamic power capture optimization and control loads reduction, a linear quadratic controller is used with a Kalman filter to minimize the criterion J_{bel}.

The LQG block scheme, based on an extended linear representation (22) is shown in Fig. 2.

The control input $T_{em}{}'$ is obtained by a linear state feedback upon the estimated state $\hat{\boldsymbol{x}}_{\boldsymbol{a}}$ via a constant gain $\boldsymbol{L}_{\boldsymbol{a}}$ resulting from the solution of the algebraic Riccati equation

$$\boldsymbol{Q}_{x_a}+\boldsymbol{P}\boldsymbol{A}_a+\boldsymbol{A}_a^T\boldsymbol{P}-\boldsymbol{P}\boldsymbol{B}_aQ_t^{-1}\boldsymbol{B}_a^T\boldsymbol{P}=\boldsymbol{0} \tag{25}$$

with

$$\boldsymbol{L}_a=Q_t^{-1}\boldsymbol{B}_a^T\boldsymbol{P} \tag{26}$$

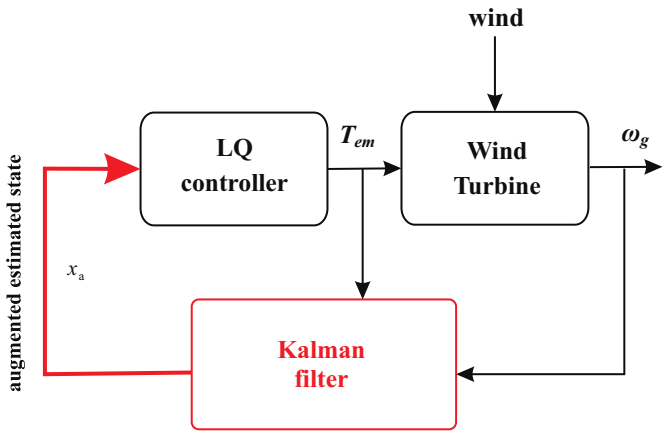

Fig. 2. LQG controller based on augmented state $\boldsymbol{x_a}$.

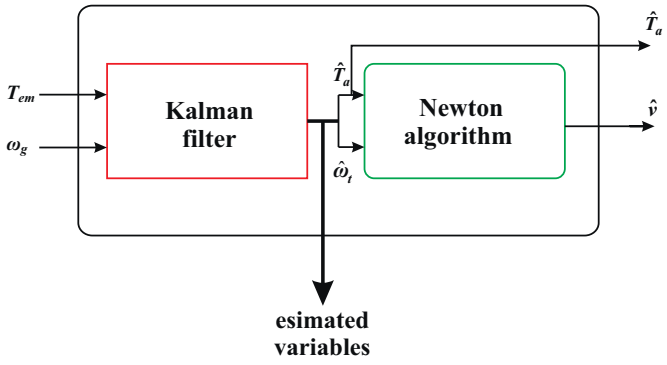

Fig. 3. Aerodynamic torque and wind speed estimator.

the control input is then,

$$T_{em} = -\boldsymbol{L}_a\hat{\boldsymbol{x}}_a + T_{em_0} \tag{27}$$

5. Wind speed estimation

The wind speed v involved in the aerodynamic equations is an effective value that cannot be directly measured. As this one is crucial to deduce the optimal rotor speed $\omega_{t_{opt}}$, a wind speed estimator is herein developed. Rather than considering the wind speed as a linear filtered non-correlated white noise, the effective wind speed is estimated using the wind turbine itself as a measurement device.

As indicated in Fig. 3, the estimator is composed of two blocks:

- A first block, that allows to estimate, from the generator speed measurement ω_g and the electromagnetic control torque T_{em}, an estimate of the aerodynamic torque $\hat{T}_a$, of the rotor speed $\hat{\omega}_t$ and the generator speed $\hat{\omega}_g$.
- A second block with, as inputs, the estimates $\hat{T}_a$ and $\hat{\omega}_t$ of the aerodynamic torque and the rotor speed respectively. The block output is the effective wind speed estimate $\hat{v}$.

The estimation of v goes through T_a one, whose estimate and also those of the other state variables are obtained using Kalman filter.

5.1. Aerodynamic torque estimation

With the aerodynamic torque as an additional state, the augmented state-space representation is then given by Eqs. (28) and (29), ξ is the process noise and v the measurement noise.

Only the generator speed, which is a noisy measurement, is assumed to be available. Generally, the state and measurement noise are assumed to be stationary, the Kalman gain matrix can then be calculated off-line. The Kalman filter considered in this work is time-invariant even if the variance of the aerodynamic torque changes over time:

$$\begin{bmatrix} \dot{\omega}_t \\ \dot{\omega}_g \\ \dot{T}_{ls} \\ \dot{T}_a \end{bmatrix} = \begin{bmatrix} -\frac{B_r}{J_r} & 0 & -\frac{1}{J_r} & \frac{1}{J_r} \\ 0 & -\frac{B_g}{J_g} & \frac{1}{n_g J_g} & 0 \\ \left(K_{ls} - \frac{B_{ls}B_r}{J_r}\right) & \frac{1}{n_g}\left(\frac{B_{ls}B_g}{J_g} - K_{ls}\right) & -B_{ls}\left(\frac{J_r + n_g^2 J_g}{n_g^2 J_g J_r}\right) & \frac{B_{ls}}{J_r} \\ 0 & 0 & 0 & 0 \end{bmatrix} \begin{bmatrix} \omega_t \\ \omega_g \\ T_{ls} \\ T_a \end{bmatrix} + \begin{bmatrix} 0 \\ -\frac{1}{J_g} \\ \frac{B_{ls}}{n_g J_g} \\ 0 \end{bmatrix} T_{em} + \begin{bmatrix} 0 \\ 0 \\ 0 \\ \xi \end{bmatrix} \tag{28}$$

$$y = [0\ \ 1\ \ 0\ \ 0] \begin{bmatrix} \omega_t \\ \omega_g \\ T_{ls} \\ T_a \end{bmatrix} + v \tag{29}$$

5.2. Wind speed computation

The estimate of the wind speed $\hat{v}$ is related to the one of $\hat{T}_a$ by the following equation:

$$\hat{T}_a - \frac{1}{2}\rho\pi R^3 C_q\left(\frac{\hat{\omega}_t R}{\hat{v}}\right)\hat{v}^2 = 0 \tag{30}$$

where $C_q(\hat{\lambda}) = C_q(\hat{\lambda}, \beta_{opt})$ is a tabulated function of $\hat{\lambda}$. In order to use a numerical method for Eq. (30) solved with respect to $\hat{v}$, this function is interpolated with a polynomial in λ

$$C_q(\lambda) = \sum_{i=0}^{n} \alpha_i \lambda^i \tag{31}$$

The Newton–Raphson algorithm, detailed in Appendix A, is then used to calculate $\hat{v}$. This value is exploited to deduce the optimal rotor speed $\hat{\omega}_{t_{opt}} = \lambda_{opt}/\hat{v}R$.

6. Nonlinear state feedback control

In order to improve the linear controller performance, the nonlinear dynamic aspect of the two-mass model must be taken into consideration. A nonlinear control strategy is then adopted based on a wind speed estimator.

6.1. Nonlinear static state feedback control

Starting from $\dot{\omega}_t$ expression

$$\dot{\omega}_t = \frac{1}{J_r}T_a - \frac{B_r}{J_r}\omega_t - \frac{1}{J_r}T_{ls} \tag{32}$$

one may deduce the second time derivative $\ddot{\omega}_t$ of the rotor speed

$$\ddot{\omega}_t = \frac{1}{J_r}\dot{T}_a - \frac{B_r}{J_r}\dot{\omega}_t - \frac{1}{J_r}\dot{T}_{ls} \tag{33}$$

it is also possible to extract $\dot{T}_{ls}$ from (9)

$$\dot{T}_{ls} = a_{31}\omega_t + a_{32}\omega_g + a_{33}T_{ls} + b_{31}T_a + b_{32}T_{em} \tag{34}$$

Replacing (32) and (34) in (33), it comes out that

$$\ddot{\omega}_t = \frac{\dot{T}_a}{J_r} - \frac{(B_r + b_{31}J_r)}{J_r^2}T_a + \frac{(B_r^2 - a_{31}J_r)}{J_r^2}\omega_t - \frac{a_{32}}{J_r}\omega_g + \frac{(B_r - a_{33}J_r)}{J_r^2}T_{ls} - \frac{b_{32}}{J_r}T_{em} \quad (35)$$

Let ε_ω be the tracking error defined as

$$\varepsilon_\omega = \omega_{t_{opt}} - \omega_t \quad (36)$$

One imposes a second order dynamics to ε_ω as

$$\ddot{\varepsilon}_\omega + b_1\dot{\varepsilon}_\omega + b_0\varepsilon_\omega = 0 \quad (37)$$

b_0 and b_1 are chosen such that the polynomial $s^2 + b_1 s + b_0$ is Hurwitz.

Replacing $\dot{\omega}_t$ given by (32) and $\ddot{\omega}_t$ given by (35), and substituting the state variable by their estimates, one concludes the expression of T_{em} for the nonlinear static state feedback with the estimator controller (NSSFE):

$$T_{em} = A_1\hat{\omega}_t + A_2\hat{\omega}_g + A_3\hat{T}_{ls} + A_4\hat{T}_a + A_5\dot{\hat{T}}_a + A_6(\ddot{\hat{\omega}}_{t_{opt}} + b_1\dot{\hat{\omega}}_{t_{opt}} + b_0\hat{\omega}_{t_{opt}}) \quad (38)$$

with

$$A_1 = \frac{(b_0J_r^2 - b_1B_rJ_r - a_{31}J_r + B_r^2)}{b_{32}J_r}, \quad A_2 = \frac{-a_{32}}{b_{32}}$$

$$A_3 = \frac{(B_r - b_1J_r - a_{33}J_r)}{b_{32}J_r}, \quad A_4 = \frac{(b_1J_r - b_{31}J_r - B_r)}{b_{32}J_r}$$

$$A_5 = \frac{1}{b_{32}}, \quad A_6 = \frac{-J_r}{b_{32}}$$

6.2. Nonlinear dynamic state feedback control

The static state feedback controller is unable to deal with control disturbances. In order to reject the effect of an additive constant control perturbation, a third order error tracking dynamics is imposed:

$$\overset{(3)}{\varepsilon}_\omega + b_2\ddot{\varepsilon}_\omega + b_1\dot{\varepsilon}_\omega + b_0\varepsilon_\omega = 0 \quad (39)$$

Similarly, b_0, b_1 and b_2 are chosen such that the polynomial $s^3 + b_2s^2 + b_1s + b_0$ is Hurwitz.

The time derivative of $\ddot{\omega}_t$ is obtained from (35). From (32) for $\dot{\omega}_t$ and (34) for $\dot{T}_{ls}$, one reaches $\overset{(3)}{\omega}_t$, as

$$\overset{(3)}{\omega}_t = B_1\omega_t + B_2\omega_g + B_3T_{ls} + B_4T_a + B_5\dot{T}_a + B_6\ddot{T}_a + B_7T_{em} + B_8\dot{T}_{em} \quad (40)$$

with

$$B_1 = \frac{[a_{31}J_r(B_r - a_{33}J_r) - B_r(B_r^2 - a_{31}J_r)]}{J_r^3}$$

$$B_2 = \frac{a_{32}[B_gJ_r + J_g(B_r - a_{33}J_r)]}{J_r^2J_g}$$

$$B_3 = \frac{[n_gJ_gJ_ra_{33}(B_r - a_{33}J_r) - a_{32}J_r^2 - n_gJ_g(B_r^2 - a_{31}J_r)]}{n_gJ_gJ_r^3}$$

$$B_4 = \frac{[b_{31}J_r(B_r - a_{33}J_r) + (B_r^2 - a_{31}J_r)]}{J_r^3}$$

$$B_5 = -\frac{(B_r + b_{31}J_r)}{J_r^2}$$

$$B_6 = \frac{1}{J_r}$$

$$B_7 = \frac{b_{32}J_g(B_r - a_{33}J_r) + a_{32}J_r}{J_r^2J_g}$$

$$B_8 = -\frac{b_{32}}{J_r}$$

Substituting this expression in (39) as well as $\dot{\omega}_t$ and $\ddot{\omega}_t$ given by (32) and (35) respectively, and replacing all the variable by their estimates, the control dynamics is thus

$$\dot{T}_{em} = C_1\ddot{\hat{T}}_a + C_2\dot{\hat{T}}_a + C_3\hat{T}_a + C_4\hat{\omega}_t + C_5\hat{\omega}_g + C_6\hat{T}_{ls} + C_7T_{em} + C_8(\ddot{\hat{\omega}}_{t_{opt}} + b_2\dot{\hat{\omega}}_{t_{opt}} + b_0\hat{\omega}_{t_{opt}}) \quad (41)$$

The coefficients C_i are detailed as

$$C_1 = \frac{1}{b_{32}}$$

$$C_2 = -\frac{(B_r + (b_{31} - b_2)J_r)}{b_{32}J_r}$$

$$C_3 = -\frac{[b_2J_r(B_r + b_{31}J_r) - b_1J_r^2 - b_{31}J_r(B_r - a_{33}J_r) - B_r^2 + a_{31}J_r]}{b_{32}J_r^2}$$

$$C_4 = -\frac{[B_r(B_r^2 - a_{31}J_r) - b_2J_r(B_r^2 - J_ra_{31}) + b_1B_rJ_r^2 - b_0J_r^3 - a_{31}J_r(B_r - a_{33}J_r)]}{b_{32}J_r^2}$$

$$C_5 = -\frac{a_{32}[J_rJ_g - B_gJ_r - J_g(B_r - a_{33}J_r)]}{b_{32}J_rJ_g}$$

$$C_6 = -\frac{b_1n_gJ_gJ_r^2 - n_gJ_gJ_ra_{33}(B_r - a_{33}J_r) + a_{32}J_r^2 + n_gJ_g(B_r^2 - a_{31}J_r) - b_2n_gJ_gJ_r(B_r - a_{33}J_r)}{b_{32}n_gJ_gJ_r^2}$$

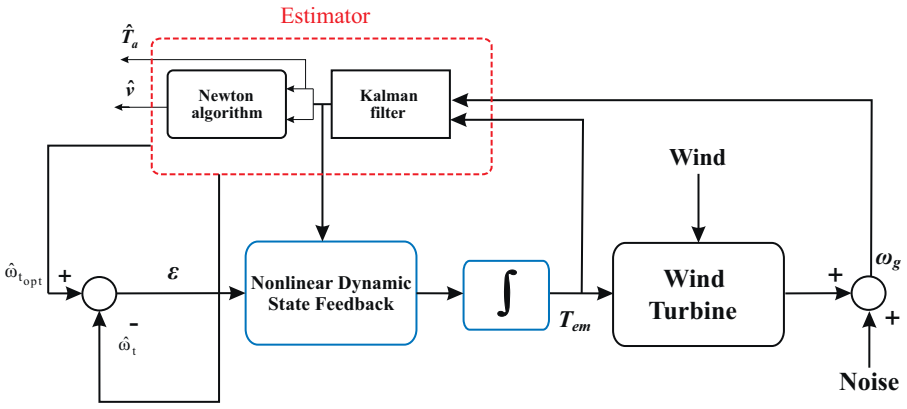

Fig. 4. Nonlinear dynamic state feedback with estimator controller scheme.

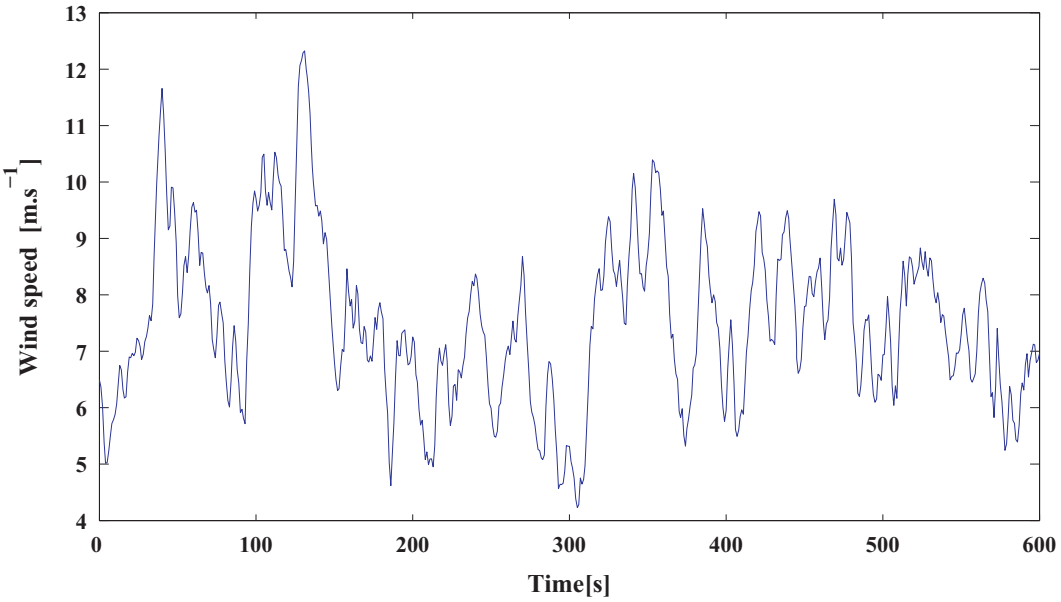

Fig. 5. Wind profile with a mean of 7 m/s.

$$C_7 = -\frac{b_3 b_2 J_r J_g - b_{32} J_g (B_r - a_{33} J_r) - a_{32} J_r}{b_{32} J_g J_r}$$

$$C_8 = -\frac{J_r}{b_{32}} \tag{42}$$

The nonlinear dynamic state feedback controller with estimator (NDSFE) scheme is shown in Fig. 4.

In order to achieve a compromise between the wind power capture optimization and control loads reduction, the following principles were adopted:

- The choice of tracking dynamics that allows to fulfill the mean tendency of the wind speed, over a given time interval, while avoiding the local high-speed variations due to the turbulence.
- The filtering of the control torque T_{em} by a low-pass filter to smooth the control input. Therefore, the drive-train is relieved from strong efforts and fast transients.
- The filtering of the rotor reference speed $\omega_{t_{opt}}$ and its derivatives to get a less turbulent reference signal.

7. Validation results

The numerical simulations were performed on a wind turbine whose characteristics are given in Table 1. These parameters correspond to the controls advanced research turbine (CART) which is located at NREL.[1] The CART is a variable-speed, variable pitch WT with a nominal power rating of 600 kW and a hub height of 36 m. It is a 43-m diameter, 2-bladed, teetered hub machine. More details about the CART wind turbine are given in Stol (2004). It is assumed to be coupled to a three-phase AC machine. Its characteristics are given in the same table. This turbine was modelled with the mathematical model and the FAST: fatigue, aerodynamics, structures, and turbulence, aeroelastic simulator for validation (Jonkman & Buhl, 2005).

In order to make a comparison between the proposed control strategies, all the simulations are carried out in the same operating conditions:

[1] NREL (National Renewable Energy Laboratory), Golden, CO.

Table 1
Wind turbine characteristics.

Rotor diameter	43.3 m
Gearbox ratio	43.165
Hub height	36.6 m
Generator system electrical power	600 kW
Maximum rotor torque	162 kN m

- Presence of constant additive control disturbance d of 10/n_g kN m (n_g=43.165).
- Presence of an additive measurement noise on ω_g with a SNR of approximatively 7 dB,
- A wind speed profile of 7 m/s, with a period of 10 mn and a turbulence intensity of I=25.00% (Fig. 5).

The instantaneous point wind speed v in the profile is the sum of two components such as

$$v = v_m + v_t \tag{43}$$

where v_m is the mean value and v_t is the turbulent component. The Van der Hooven experimental wind spectra show that the mean value v_m has a peak at a period corresponding to 10 min on average (Burton et al., 2001). For this purpose, a 10 min wind data set is chosen to keep a constant mean value. Such a period of time is then well adapted to test the developed controllers.

7.1. Using the simplified mathematical model

The proposed linear and nonlinear controllers are first tested using the simplified two-mass mathematical model with the CART parameters. Simulation results are presented in Figs. 6 and 7. As one can see in rotor speed curves (Fig. 6), the LQG controller is unable to supply a convenient control torque T_{em} for an efficient tracking of the optimal rotor speed $\omega_{t_{opt}}$. This is due to the limits of the linearized model (22) which is not longer valid under wind speed turbulence. Consequently, the produced electric power in Fig. 7 is less important with the linear controller, especially for high wind speed variations, as in between instants 300 and 400 s. Fig. 8 shows the low-speed shaft torque for both controllers.

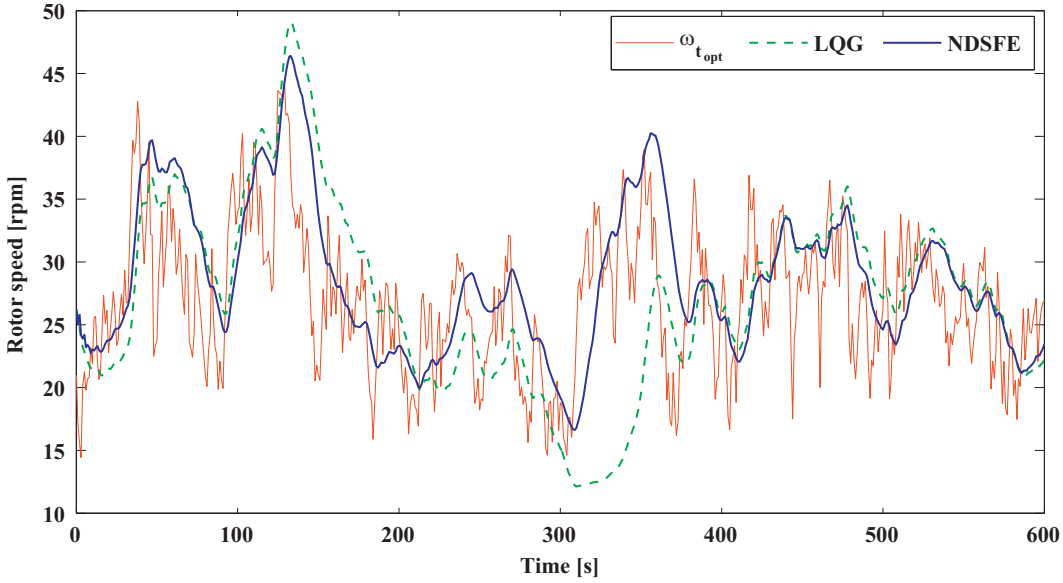

Fig. 6. Rotor speed using the two-mass mathematical model.

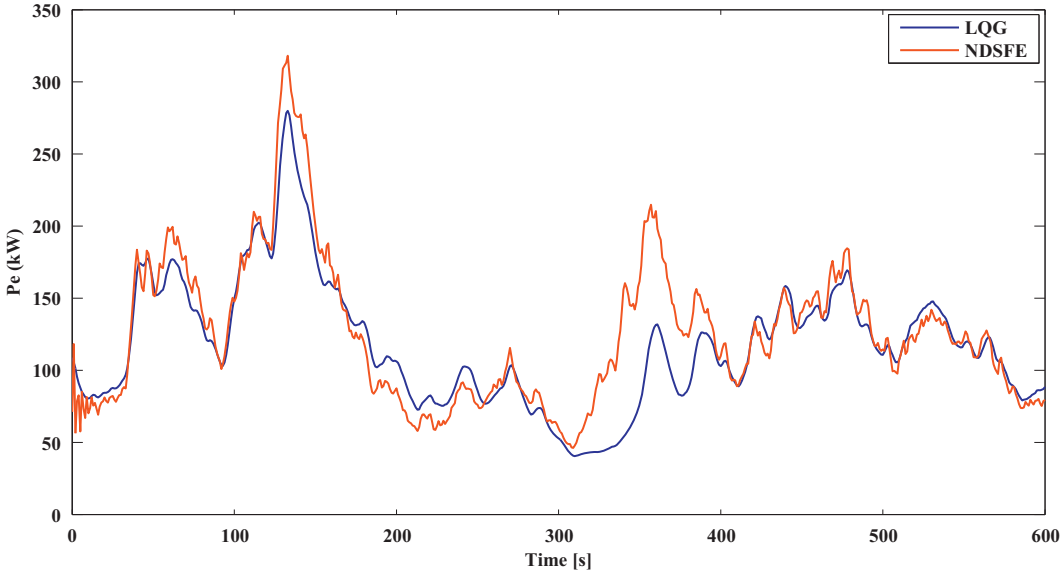

Fig. 7. Electrical power using the two-mass mathematical model.

It comes out from this figure that the nonlinear controller excites less the drive train while providing a better power capture.

7.2. Brief simulator description

In order to validate the proposed controllers, an aeroelastic wind turbine simulator is used. It allows a better representation of the WT taking into account most of the phenomena that are not modelled with the simplified mathematical model, as for instance the 3-D wind speed profile effects on the rotor blades, the flexibility of the blades, and the nonlinear behavior of the low speed shaft, modeled by a simple torsional torque with the mathematical model.

The fatigue, aerodynamics, structures and turbulence (FAST) code developed by NREL is an aeroelastic WT simulator that is capable of modelling two and three bladed propeller-type machines (Jonkman & Buhl, 2005). This code is used by WT designers to predict both extreme and fatigue loads. It uses an assumed mode method to model flexible blades and tower components. Other components are modelled as rigid bodies. In this study, three degrees-of-freedom (DOFs) are simulated: the variable generator and rotor speed (2 DOFs) and the blade teeter DOF. The variable generator and rotor speed DOFs account for the variations in generator speed and the drive train flexibility associated with torsional motion between the generator and hub/rotor. The blade teetering DOF accounts for the teeter motion induced by asymmetric wind loads across the rotor plane. FAST subroutines are coupled in an S-Function to be incorporated in a Simulink scheme. Hence, FAST is interfaced with Matlab Simulink (Fig. 9) allowing users to develop and test high performance control.

7.3. Validation using FAST

The commands thus validated using the above simulator leads to results represented in Table 2. For a better visibility, the rotor

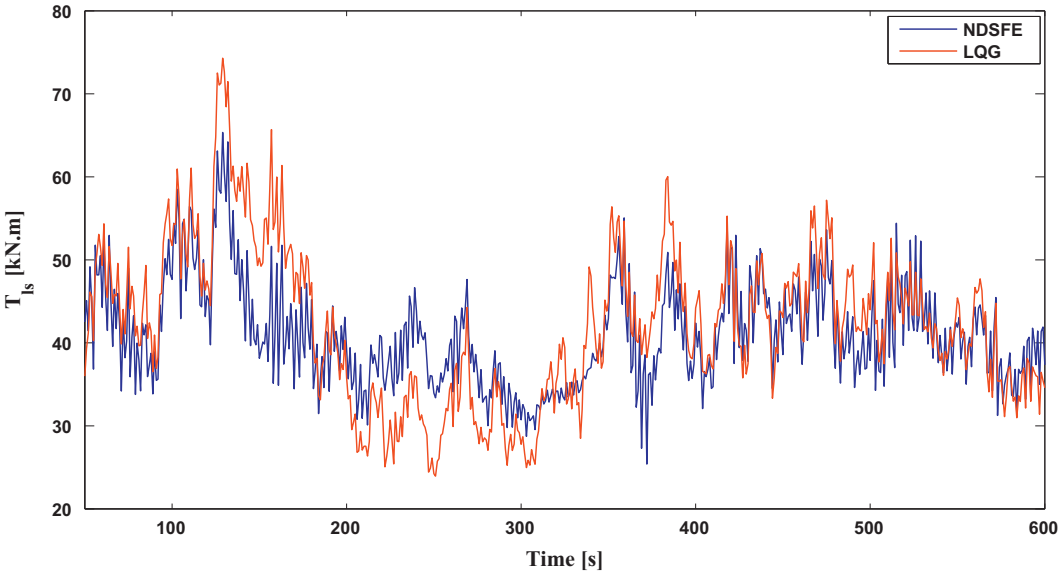

Fig. 8. Low-speed shaft torque using the two-mass mathematical model.

Table 2
Comparison of the different control strategies.

Controller	LQG	NSSFE	NDSFE
std(T_{em}) (kN m)	0.29	0.27	0.244
max(T_{em}) (kN m)	1.71	1.61	1.52
std(T_{ls}) (kN m)	12.25	10.91	9.23
max(T_{ls}) (kN m)	80.27	68.32	54.65
η_{aero} (%)	77.98	88.35	92.71
η_{elec} (%)	62.10	71.97	74.95

speed ω_t, the electromagnetic torque T_{em}, the low-speed shaft torque T_{ls} and the electrical power are gathered, for each applied controller, on the same chart.

The rotor speed ω_t is shown in Fig. 10. For the LQG controller parameters tuning, to minimize the J_{bel} criterion (23), only the ratio between the two tuning parameters Q_a and Q_t of the LQG controller is relevant, therefore, in order to bring acceptable control loads reduction, Q_a is fixed to 1 and Q_t to 0.05.

One can observe that the LQG controller achieves a rotor speed that is below the optimal speed $\omega_{t_{opt}}$. Refereing to the wind speed profile, one can also observe that this deviation is more significant during high-turbulence time periods. This is due to the failure of the LQG controller to reject the perturbation on the control torque and the consideration of the dynamical aspect of the wind.

The constants b_0 and b_1 of the NSSFE characteristic polynomial are fixed to 0.0055 and 0.1333 respectively. The constants b_0, b_1 and b_2 of the NDSFE are 0.1, 0.8 and 1.7 respectively. These choices are made in order to ensure a time response of about 20 s for the tracking dynamic. Due to the input disturbance effect, the nonlinear static state feedback with estimator controller ensures a rotor speed that is either below or above the optimal rotor speed $\omega_{t_{opt}}$. Oppositely, the nonlinear dynamic state feedback with estimator controller achieves a regular tracking of the mean tendency of the optimal rotor speed during all the simulation time. The deviation from the optimal reference is reflected on the power capture. Referring to Fig. 11 that represents both optimal $P_{a_{opt}}$ and captured P_a aerodynamic power, the NDSFE controller ensures a better aerodynamic power capture than the LQG one. The same observation can be made concerning the produced electrical power (Fig. 12). The NDSFE controller achieves a largely better performance than the LQG one. This performance is also better than the one reached by NSSFE controller. According to Table 2, the aerodynamic efficiency η_{aero} of the LQG controller is 14% less than the NDSFE one. The gap in the electrical efficiency η_{elec} is in the same order of magnitude, that is around 13%. This is due to the weak control torque of the LQG controller that cannot ensure a good compromise between power capture and load reductions.

The controllers efficiency is compared using two criteria: the aerodynamic η_{aero} and the electrical η_{elec} efficiency. They are defined as

$$\eta_{\text{aero}}(\%) = \frac{\int_{t_{ini}}^{t_{fin}} P_a \, \mathrm{d}t}{\int_{t_{ini}}^{t_{fin}} P_{a_{opt}} \, \mathrm{d}t}, \quad \eta_{\text{elec}}(\%) = \frac{\int_{t_{ini}}^{t_{fin}} P_e \, \mathrm{d}t}{\int_{t_{ini}}^{t_{fin}} P_{a_{opt}} \, \mathrm{d}t} \tag{44}$$

where $P_{a_{opt}} = \frac{1}{2}\rho\pi R^2 C_{p_{opt}} v^3$ is the optimal aerodynamic power corresponding to the wind speed profile and P_e is the electrical power. The low-speed shaft torsion and control torque minimization are evaluated by their variance and maximum.

The electromagnetic control torque is presented in Fig. 14. Refereing to Table 2, the maximal T_{em} value is around 1.71 kN m with the LQG controller. Even though it ensures the best power capture performance, the NDSFE needs the lowest maximum T_{em} value, compared to all the controllers, of 1.5 kN m. Similarly with the T_{em} standard-deviation, that is the lowest with the NDSFE controller and the highest with the LQG one.

Figs. 12 and 13 show that the NDSFE controller is able to fulfill a good compromise between produced electrical power maximization and low speed shaft torsional oscillation minimization. The produced electrical power is higher than for all controllers. According to Table 2, the low speed shaft torque T_{ls} mean value and standard-deviation are lower with the NDSFE controller than the LQG and NSSFE ones.

In fact, Fig. 13 shows that the stress submitted by the low speed shaft is greatly reduced with the nonlinear dynamic controller.

8. Conclusion

Linear and nonlinear controllers based on a flexible two-mass model of wind turbine drive train were proposed in this work for wind power capture optimization. They take into consideration the flexibility of the low speed shaft. The proposed linear and nonlinear controllers are first tested using the simplified

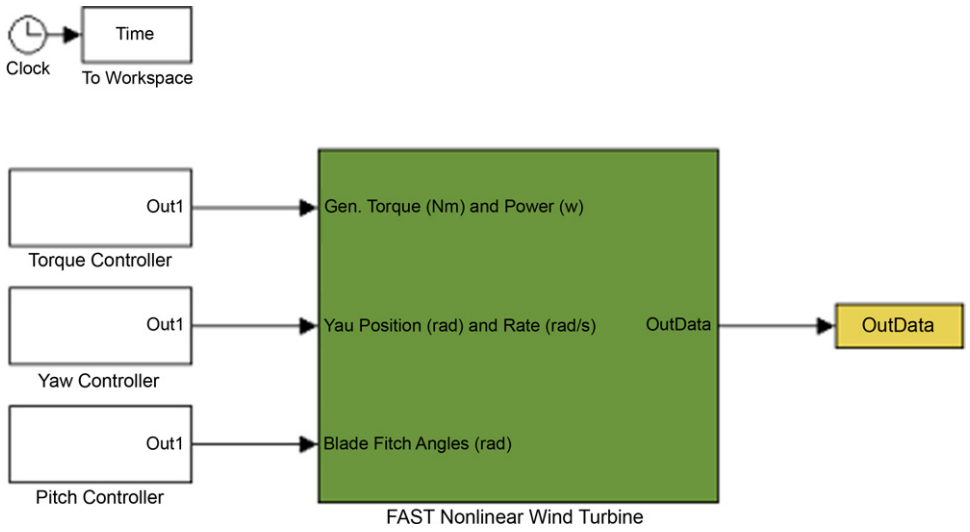

Fig. 9. Fast simulink block.

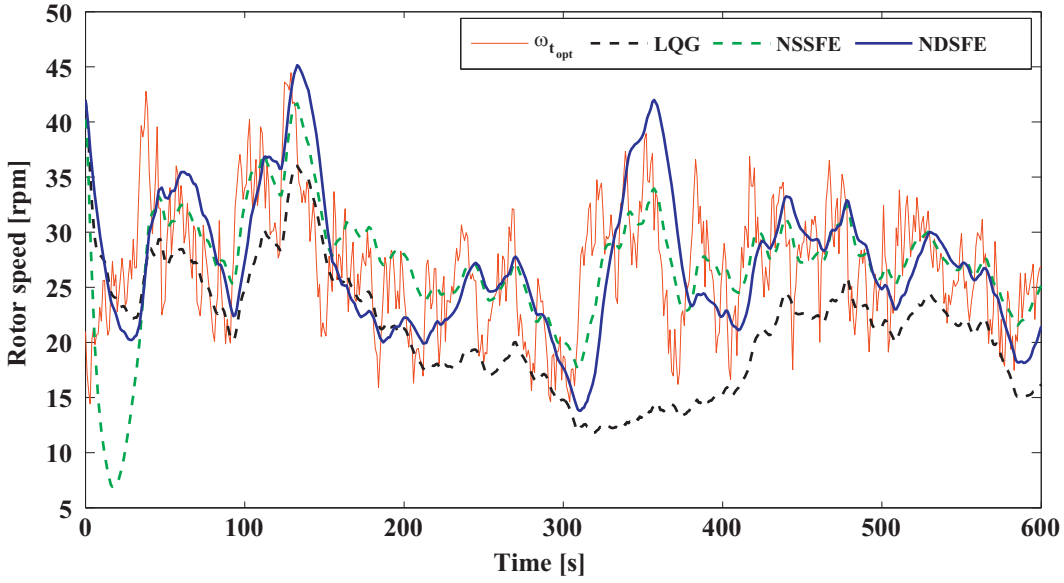

Fig. 10. Rotor speed with FAST simulator.

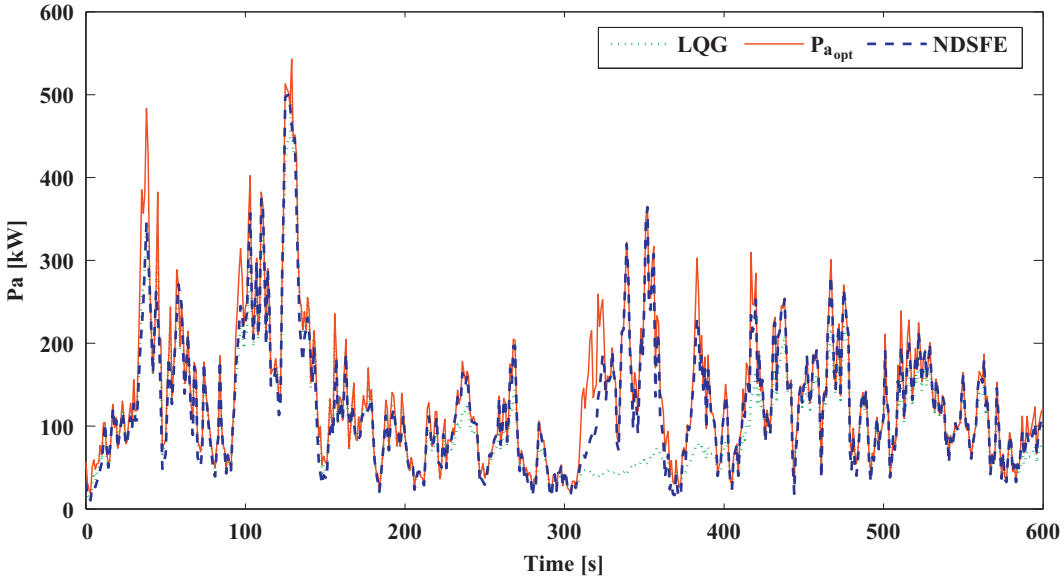

Fig. 11. Aerodynamic power with FAST simulator.

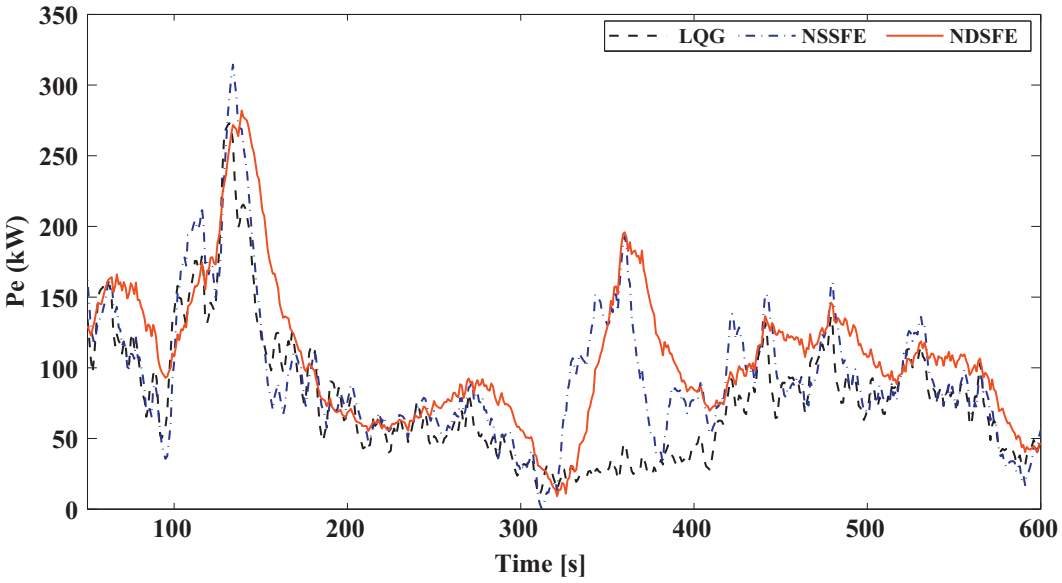

Fig. 12. Electrical power with FAST simulator.

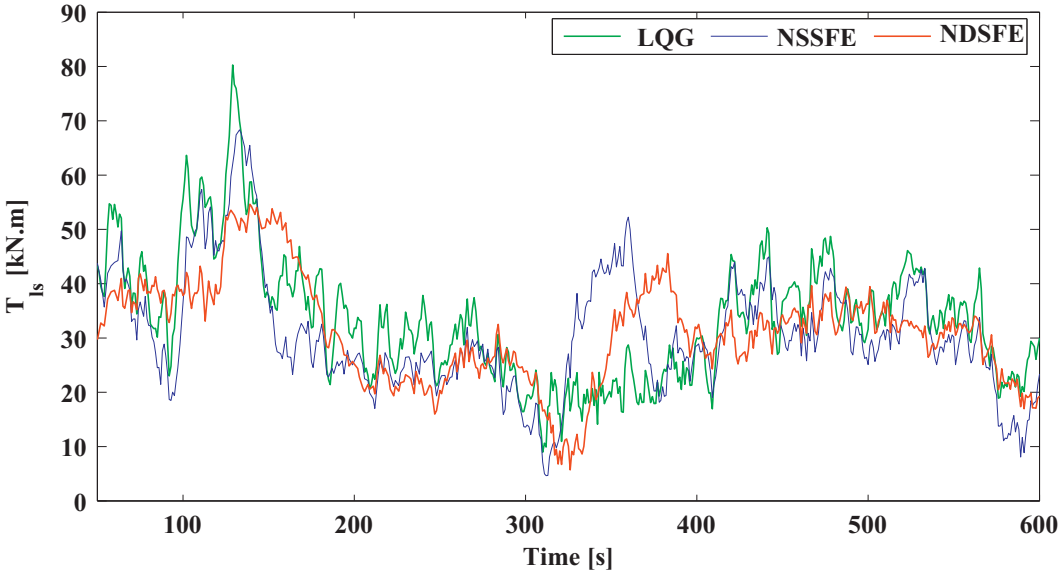

Fig. 13. Low-speed shaft torque with FAST simulator.

two-mass mathematical model with the parameters of a real experimental wind turbine. After that, they are validated using an aeroelastic wind turbine simulator.

The linear LQG controller is not able to achieve good performance, especially for high-turbulence wind speeds. A nonlinear dynamic state feedback controller is then designed based on the nonlinear two-mass model. The nonlinear dynamic controller outperform the LQG one with both the simplified and the FAST model and fulfill a good compromise between power capture optimization and drive train loads reduction.

Appendix A. Wind speed estimation algorithm

For a given instant t, the effective wind speed $\hat{v}(t)$ is obtained using Newton algorithm from the aerodynamic torque estimate $\hat{T}_a(t)$ and the rotor speed estimate $\hat{\omega}_t(t)$ given below the Kalman filter as described in Section 5. The iterative form of the algorithm is described below

Algorithm 1. Calculate $v = \hat{v}(t)$.

Require: $N > 0$, $\varepsilon_{min} > 0$, $\hat{T}_a(t)$,$\hat{\omega}_t(t)$ and $\hat{v}(t-T_s)$
Ensure: $v = \hat{v}(t)$
$v \Leftarrow \hat{v}(t-T_s)$
$n \Leftarrow 0$
repeat
  $\lambda_n = \frac{\hat{\omega}_t(t)R}{v}$
  $H_n \Leftarrow -\rho\pi R^3 C_q(\lambda_n)v + \frac{1}{2}\rho\pi R^4 \hat{\omega}_t(t)\frac{\partial C_q(\lambda)}{\partial \lambda}$
  $g_n \Leftarrow \hat{T}_a(t) - \frac{1}{2}\rho\pi R^3 C_q(\lambda_n)v_n^2$
  $v_{old} \Leftarrow v$
  $v \Leftarrow v - H_n^{-1} \cdot g_n$
  $n \Leftarrow n+1$
until $(n \geq N)$ or $(\frac{v-v_{old}}{v} \leq \varepsilon_{min})$
return v

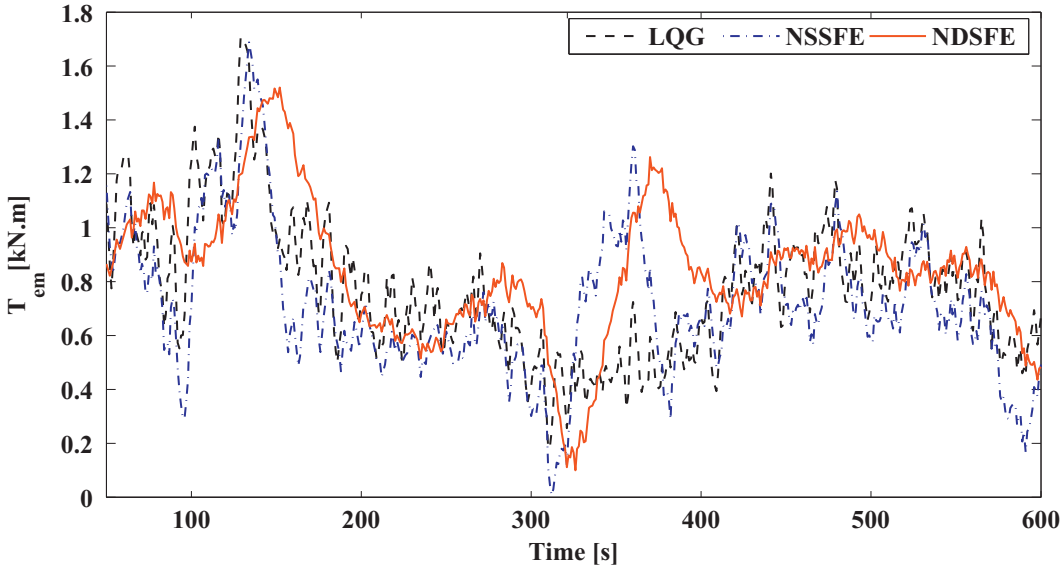

Fig. 14. Electromagnetic torque with FAST simulator.

Appendix B. Two-mass model parameters

Rotor radius	$R=21.65\,\mathrm{m}$
Air density	$\rho=\mathrm{kg/m^3}$
Rotor inertia	$J_r=3.25\times10^5\,\mathrm{kg\,m^2}$
Generator inertia	$J_g=34.4\,\mathrm{kg\,m^2}$
Shaft damping coefficient	$B_{ls}=9500\,\mathrm{N\,m/rad/s}$
Shaft stiffness coefficient	$K_{ls}=2.691\times10^5\,\mathrm{N\,m/rad}$
Rotor friction coefficient	$B_r=27.36\,\mathrm{N\,m/rad/s}$
Generator friction coefficient	$B_g=0.2\,\mathrm{N\,m/rad/s}$
Gearbox ratio	$n_g=43.165$

References

Anderson, B., & Moore, J. (1989). *Optimal control: Linear quadratic methods*. Prentice-Hall.

Bianchi, F. D., Battista, H. D., & Mantz, R. J. (2006). *Wind turbine control systems: Principles modelling and gain scheduling design* (2nd ed.). Springer.

Bianchi, F. D., Mantz, R. J., & Christiansen, C. F. (2005). Gain scheduling control of variable-speed wind energy conversion systems using quasi-LPV models. *Control Engineering Practice*, *13*(2), 247–255.

Bongers, P. M. M. (1994). *Modeling and identification of flexible wind turbines and a factorizational approach to robust control*. Ph.D. thesis, Delft University of Technology, June.

Bongers, P. M. M., Bierbooms, W., Dijkstra, W., & van Hoten, T. (1990). *An integrated dynamic model of a flexible wind turbine*. Technical Report, Delft University of Technology.

Boukhezzar, B., Lupu, L., Siguerdidjane, H., & Hand, M. (2007). Multivariable control strategy for variable speed, variable pitch wind turbines. *Renewable Energy*, *32*(8), 1273–1287.

Boukhezzar, B., & M'Saad, M. (2008). Robust sliding mode control of a DFIG variable speed wind turbine for power production optimization. In *16th Mediterranean conference on control and automation* (pp. 795–800).

Boukhezzar, B., & Siguerdidjane, H. (2009). Nonlinear control with wind estimation of a dfig variable speed wind turbine for power capture optimization. *Energy Conversion and Management*, *50*(4), 885–892.

Boukhezzar, B., Siguerdidjane, H., & Hand, M. (2006). Nonlinear control of variable-speed wind turbines for generator torque limiting and power optimization. *ASME Journal of Solar Energy Engineering*, *128*(4), 516–530.

Burns, R. (2001). *Advance control engineering*. Buterworth-Heinemann.

Burton, T., Sharpe, D., Jenkins, N., & Bossanyi, E. (2001). *Wind energy handbook*. John Wiley & Sons.

Camblong, H. (2008). Digital robust control of a variable speed pitch regulated wind turbine for above rated wind speeds. *Control Engineering Practice*, *16*(8), 946–958.

Ekanayake, J. B., Holdsworth, L., Wu, X. G., & Jenkins, N. (2003). Dynamic modelling of doubly fed induction generators wind turbines. *IEEE Transaction on Power Systems*, *18*(2), 803–809.

Ekelund, T. (1997). *Modeling and linear quadratic optimal control of wind turbines*. Ph.D. thesis, Chalmers University of Technology, Sweden.

Ekelund, T., & Schmidtbauer, B. (1993). Tradeoff between energy capture and dynamic loads in variable speed wind turbines. In *Proceedings of the IFAC 12th world congress*, Vol. 7 (pp. 521–524).

Ekelund, T., & Schmidtbauer, B. (1994). Trade-off between energy capture and dynamic loads in variable speed wind turbines. *Control Engineering Practice*, *2*(6), 1078.

Ernst, J., & Leonhard, W. (1985). Optimisation of wind energy output of variable speed wind turbines. In *Wind power 85*, San Francisco, CA.

Heier, S. (1998). *Grid integration of wind energy conversion systems*. John Wiley & Sons Ltd.

Jonkman, J. M., & Buhl, M. L. (2005). *FAST USER's GUIDE* (6th ed.). National Wind Technology Center, National Renewable Energy Laboratory, Golden, CO.

Lin, F. (2007). *Robust control design: An optimal control approach*. John Wiley & Sons.

Ma, X. (1997). *Adaptive extremum control and wind turbine control*. Ph.D. thesis, Denmark, May.

Munteanu, I., Bratcu, A. I., Cutululis, N.-A., & Ceang, E. (2008). *Optimal control of wind energy systems: Towards a global approach*. Springer-Verlag.

Munteanu, I., Cutululis, N., Iuliana, A., & Ceanga, E. (2005). Optimization of variable speed wind power systems based on a LQG approach. *Control Engineering Practice*, *13*(7), 903–912.

Novak, P., Jovik, I., & Schmidtbauer, B. (1994). Modeling and identification of drive-system dynamics in a variable-speed wind turbine. In *Proceedings of the third IEEE conference on control applications*, Vol. 1.

Sørensen, P., Hansen, A. D., Janosi, L., Bech, J., & Bak-Jensen, B. (2001). *Simulation of interaction between wind farm and power systems*. Risø Report R-1281(EN), Risø National Laboratory, Roskilde, Denmark.

Stol, K. A. (2004). *Geometry and structural properties for the controls advanced research turbine (CART) from model tuning*. Subcontractor Report SR-500-32087, National Renewable Energy Laboratory, Golden, CO, September.

Van der Hooft, E. L., & Van Engelen, T. G. (2003). *Feed forward control of estimated wind speed*. Technical Report ECN-C-03-137, ECN Windenergie, December.

Van der Hooft, E. L., & Van Engelen, T. G. (2004). Estimated wind speed feed forward control for wind turbine operation optimisation. In *European wind energy conference proceedings*, London.

Vihriälä, H. (2002). *Control of variable speed wind turbines*. Ph.D. thesis, Tampere University of technology, November.